

Study of Fluid Flow on a Flat Plate with Multiple Rectangular Impinging Slot Jets

Malladi R.Ch. Sastry^{#1}, B. V. S. S. S. Prasad^{*2}, A.V.S.S.K.S Gupta^{#3}

[#]Associate Professor, Dept. of Mechanical Engg., Gudlavalleru Engg. College, Gudlavalleru, India.

^{*}Professor, Thermal Turbo Machines Laboratory, Dept. of Mechanical Engg., IITM, Chennai, India.

[#]Professor, Dept. of Mechanical Engineering, JNTU College of Engineering, Hyderabad, India.

Abstract – Computational and experimental studies on a flat plate are conducted by an array of five rectangular air jets impinging on its top surface. The array jet consists of a central jet surrounded by four neighboring perimeter jets. Computations are carried out by Shear Stress Transport (SST) κ - ω turbulence model. The jet-to-plate spacing (H) to hydraulic diameter of slot (D) ratio is varied from 0.5 to 4 and jet Reynolds number is varied from 5282 to 8450. The computationally obtained flow structure reveals the complex interaction of the wall jets. Primary pressure peaks are observed at the stagnation point and the secondary peaks are noticed at the interaction points of the wall jets. Position of the secondary peaks depends upon H/D and is independent of Reynolds number, whereas the size of the peak depends upon both H/D and Reynolds number.

Keywords – Jet impingement, array jet, flow visualization, Experiments, CFD

1 INTRODUCTION

Jet impingement flows are frequently used in various industrial applications for their superior heat and mass transfer characteristics compared to those obtained for the same amount of gas flowing parallel to the target surface. Impinging jets are extensively used in diverse industrial applications because of their highly attractive local heat transfer characteristics. Industrial applications include tempering of glass, drying of paper and textiles, annealing of non ferrous metal sheets, cooling of turbine blades, and cooling of microelectronic components. Although such jets yield very high heat transfer coefficients in the stagnation zone, the cooling performance drops rapidly away from the impingement zone. For this reason jets are often used in arrays in industrial practice. In such cases interaction between the jets in the array plays an important role in the cooling performance. The collision of wall jets after impingement produces a complex flow field. The ability to control heat transfer from the surface by varying flow parameters such as jet exit velocity and geometrical parameters such as jet exit opening, jet-to-plate spacing, and nozzle-to-nozzle spacing in arrays are some of the key factors that have lead to the sustained and widespread use of jet impingement technology. The most commonly used geometries are axisymmetric (circular orifice or pipe), slot (two-dimensional) nozzles, rectangular (three-dimensional) and square (three-dimensional) nozzles. San et al., 2001 and 2007, and Aldabbagh and Sezai (2002) have investigated numerically

the flow and heat transfer characteristics of impinging laminar multiple square jets, showed that more uniform heat transfer can be obtained by using shower head type impinging on the surface. Most recent review articles on this topic are provided by Bernhard et al., 2009 reviewed the flow and heat transfer characteristics of multiple impinging jets and compared with single impinging jets. Prasad et al, 2011 reported the effect of jet-to-plate spacing to jet diameter ratio (H/D) and Reynolds number on the pressure distribution and flow structure for circular jets impinging on a flat surface.

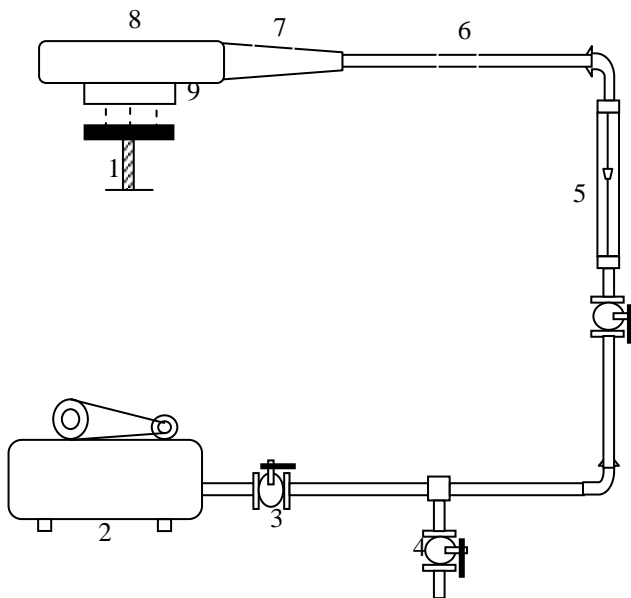
The broad objectives of the paper are therefore to computationally investigate (i) the flow structure of the interacting jets (ii) the effect of varying H/D and Reynolds number on pressure distribution. Flow visualization experiments with oil-lampblack technique are carried out to qualitatively corroborate the computational flow structure with visualized patterns. Similarly the computational pressure distributions are compared with experimental data.

2 EXPERIMENTAL DETAILS

The schematic layout of the experimental set up is shown in Fig.1. Air is supplied by a reciprocating air compressor through a calibrated Rotameter. Flow regulating and bypass valves are placed in supply line to control the flow rate. Air enters into the plenum chamber through diverging section to reduce the pressure fluctuations in air.

A seamless rectangular chamber of 600 mm length, 300 mm width, 300 mm height and 6 mm thickness, is used as plenum chamber, whose size is large enough to stabilize the flow and reduce the fluctuations. Air from plenum chamber enters into the impingement air chamber which is made of 160 mm length, 160 mm width, 160 mm height and 4mm thick square chamber.

The exit side of the impingement air chamber is a semi-confining plate, which contains five rectangular orifices of dimensions 6×12 mm. Air ejects as jet through the orifices and impinges on the target surface. Around the centre jet, the four perimeter jets are placed at 90° apart from each other. Distance between the centre jet and perimeter jets are maintained 32mm. Air ejects as jet through the orifice and impinges on the target surface.



- (1) Test section (2) Compressor (3) Flow control valve
- (4) Bypass line (5) Rotameter (6) Hoss pipe
- (7) Diverging section (8) Plenum chamber
- (9) Impingement chamber

Fig. 1 Schematic diagram of experimental set-up

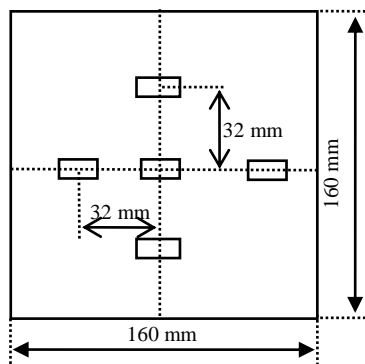


Fig.2 Semi-confining plate with Dimensions

The impingement plate is of five millimeter thick acrylic sheet of 160 × 160 mm is used. In order to determine the static pressure distribution on the target surface, a close array of pressure tap holes of 0.8 mm diameter are drilled along the length of plate. The tap holes are closely placed because of the steep change of pressure expected due to jet interactions. Multi tube manometer is used for wall static pressure measurement. Impingement plate is placed over a stand, whose height can be varied by a lead screw mechanism to obtain the required H/D ratio.

Flow visualization experiments are carried out with oil-lampblack technique. The oil and lampblack powder are mixed in proper proportion and painted on the target surface. The lampblack coated target surface is kept beneath the impingement chamber. The air jets, after impinging on the

target surface, leave traces of the flow path lines on the plate. These pictures are captured by a camera.

3 COMPUTATIONAL METHODOLOGY

Figure 3 shows the geometric model that mimics the physical model used for experiment of interest. It consists of a semi-confined plate and 160 × 160 mm square impingement plate. The semi-confining plate consists of five rectangular jets each of 6 × 12 mm in size. The jet ejects from the rectangular orifice to impinge on the target surface. Distance between the impingement plate and the jet exit is varied to obtain the H/D ratio from 0.5 to 4.

The computational mesh suitable for finite volume method is generated by automatic grid generating tool GAMBIT 2.3.16. Non-uniform grids with clustered nodes are generated in the regions where steep gradient of velocity is expected. Optimum grid size is selected after the grid independence study.

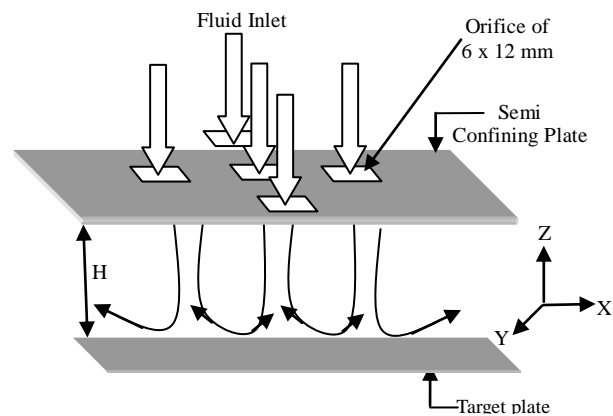


Fig. 3 Schematic diagram of the geometry and boundary conditions

For the purpose of computation, a specified mass flow inlet condition is imposed at the entry to the orifice. The jet after hitting the plate, exits into the atmosphere in the transverse direction all around the plate periphery, where constant (ambient) pressure outlet condition is imposed. All the input values imposed are those used in the experiment.

The three dimensional flow is formulated with the following assumptions: (i) the fluid is incompressible, (ii) the fluid properties are constant and (iii) the flow is steady. The governing equations used for simulations are the Reynolds averaged continuity and momentum equations for modeling the turbulence quantities.

A finite volume based solver Fluent 6.3 is used for solving the governing continuity, momentum and turbulence-model equations. SIMPLE algorithm is used for pressure velocity coupling. The solution is considered to be converged when the residual is in the order of 10^{-6} for continuity, momentum and turbulence equations. The $\kappa-\omega$ SST model is adopted for simulation.

Continuity equation,

$$\nabla \cdot (\rho u) = 0 \quad (1)$$

Momentum equation,

$$(u \cdot \nabla)u - \frac{1}{\rho} \nabla p + \nu \nabla^2 u = 0 \quad (2)$$

Turbulent kinetic energy (K) equation,

$$\frac{\partial(\rho k u_i)}{\partial x_i} = \frac{\partial}{\partial x_j} \left(\Gamma_k \frac{\partial k}{\partial x_j} \right) + \bar{G} \bar{G}_k - Y_k + S_k \quad (3)$$

Specific dissipation rate (ω) equation

$$\frac{\partial}{\partial x} (\rho \omega u_i) = \frac{\partial}{\partial x_j} \left(\Gamma_\omega \frac{\partial \omega}{\partial x_j} \right) + \bar{G} \omega - Y_\omega + S_\omega \quad (4)$$

Where

$$\Gamma_k = \mu + \frac{\mu_k}{\sigma_k}, \quad \Gamma_\omega = \mu + \frac{\mu_t}{\mu_\omega}, \quad \sigma_{k,1} = 1.176,$$

$$\sigma_{\omega,1} = 2.0, \sigma_{k,2} = 1.0, \sigma_{\omega,2} = 1.168$$

Boundary conditions used for the present study are,

(i) No slip boundary condition

$$V_w = 0, \text{ at } z = 0$$

(ii) Flow inlet condition,

$$V_x, V_y = 0, V_z = V_{oe}$$

(iii) Entrainment condition,

$$P = P_{atm}$$

The parameters investigated in the present study include (i) effect of H/D, varied as 0.5, 1, 2 and 4 (ii) effect of jet exit Reynolds number, varied as 5282, 6340, 7395 and 8450.

3.1 Mesh sensitivity

Mesh sensitivity study is carried out to ascertain the accuracy of the numerical results. The mesh sensitivity study is carried out by analyzing the variation of static pressure distribution on the target plate along line A-A for H/D = 2 at Re 6340 as shown in Table 1. It is clear from the table that variation in the value of static pressure with 1.691 million and 1.995 million size is not significant. To get advantage of computational time, mesh size of 1.691 million is used for this case. Similar mesh sensitivity study is done for all other cases.

TABLE 1
MESH SENSITIVITY

| Mesh Size in Million cells | Static Pressure (Pa) |
|----------------------------|----------------------|
| 0.8 | 151.2 |
| 1.02 | 157.6 |
| 1.691 | 162.4 |
| 1.995 | 162.8 |

3.2 Data Reduction

Numerical results are obtained after solving the governing equations. The results are presented in non dimensional form. The pertinent dimensionless parameters appearing in the problem are: Reynolds number, H/D, X/D and non-dimensional pressure coefficient.

The non-dimensional pressure coefficient (P^*) is defined as the ratio of static pressure at particular location to the maximum static pressure for the case in function. The non-

dimensional pressure coefficient is drawn along lines A-A and B-B. Figure 4 shows the lines selected for plotting the results.

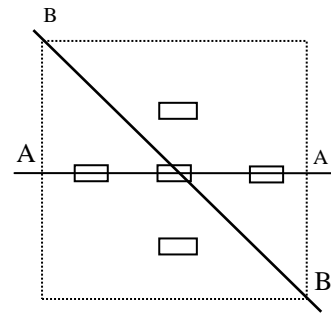


Fig. 4 lines selected for plotting results

4 RESULTS AND DISCUSSION

4.1 Flow Structure of Impinging Jet:

As the fluid ejects out of the orifice into the quiescent ambient, a continuous reduction in velocity takes place from the centre jet to its boundary. With increasing distance from the exit, momentum exchange between jet and the ambient broadens the free boundary of the jet whilst the potential core contracts. At the impingement plane the wall jets are formed. The wall jets emanating from each impinging jet forms a collision front due to its interaction with neighbors. Consequently an up-wash flow fountain flow with a dividing stagnation line takes place. Figure 5 shows the computed velocity contours of the impinging jet along two planar surfaces A-A and B-B. Plane A-A passes through the perimeter and center jet, where as plane B-B passes through along protruded corners of the centre jet.

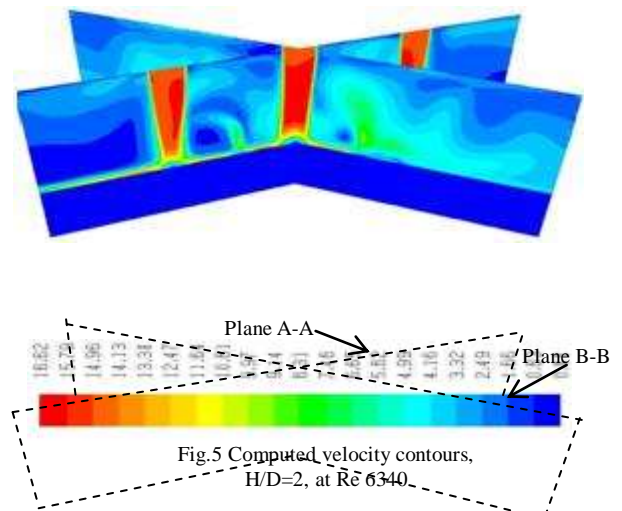


Fig.5 Computed velocity contours, H/D=2, at Re 6340

Figure 6 shows the velocity contours for the four jet-to-plate spacing to hydraulic diameter of slot ratio namely H/D = 0.5, 1, 2, 4 for Reynolds number 6340. It can be clearly seen that in case of H/D = 0.5 & 1 the potential core is extended up to target surface shown in Fig.6 (a&b). Where as in case of H/D = 2 & 4

the potential core region vanishes by the time flow reaches the target surface, shown in Fig.6 (c&d). These differences in velocity pattern happen because of the variation in momentum exchange between the fluid jet and ambient. Fig.7 shows velocity contours along the plane B-B.

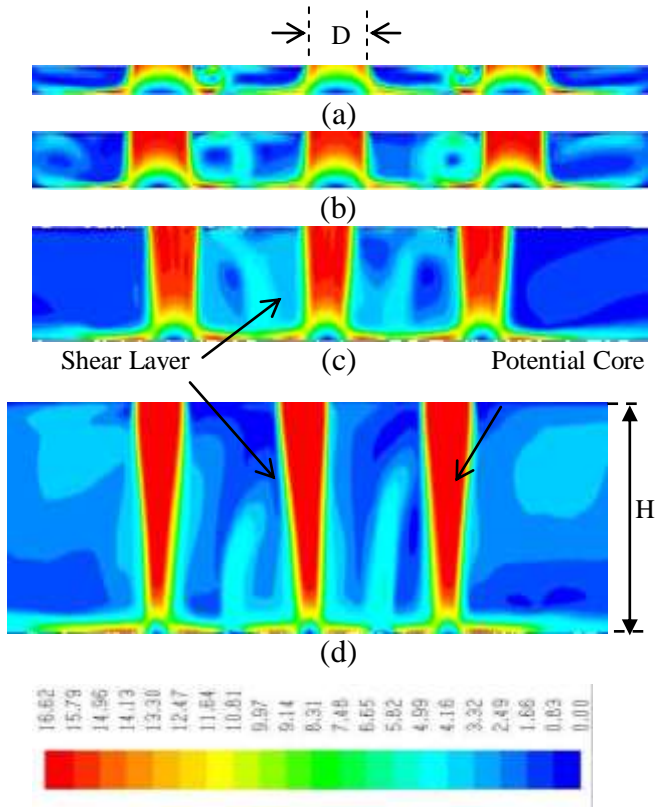


Fig. 6 Computed Velocity Contours Along Plane A-A, For Re = 6340
(a) H/D=0.5 (b) H/D=1 (c) H/D=2 (d) H/D=4

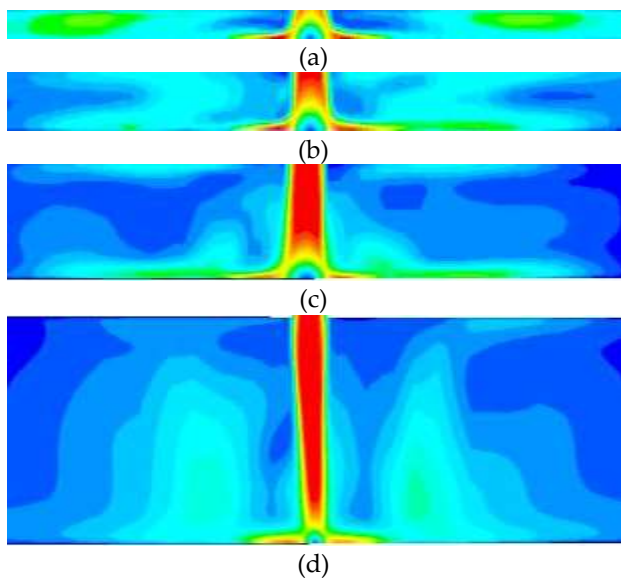


Fig. 7 Computed Velocity Contours Along Plane B-B, For Re = 6340
(a) H/D=0.5 (b) H/D=1 (c) H/D=2 (d) H/D=4

Figure 8 shows the path lines coloured by velocity. The wall jets from adjacent jets when interacts with each other an upwash flow takes place as shown in Fig.8. When H/D value is lower (H/D=0.5 & 1) the interaction is prominent, besides as the distance is less the upwash flow fountain reaches the semi-confinement plate.

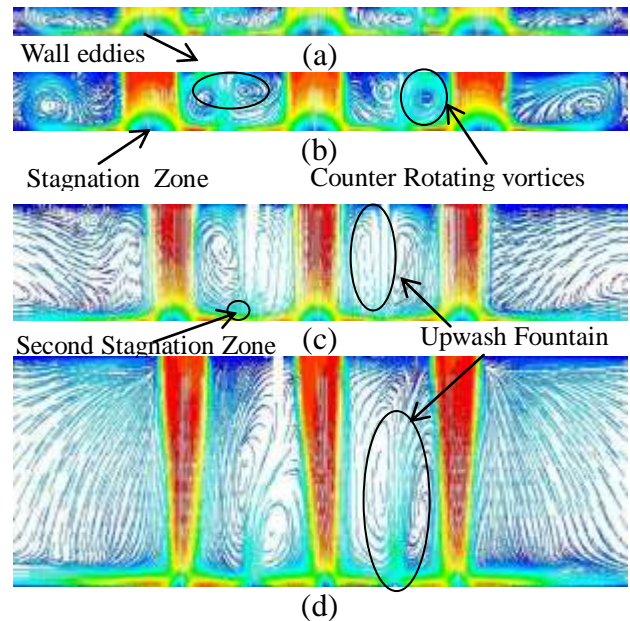
This low velocity jet forms another wall jets on the semi-confining plate, shown in Fig. 8 (a & b).

But no such thing happens for higher H/D, because the second jet diffuses out by the time it reaches the top surface, shown in Fig.6 (c & d). It is observed that the position of the attachment line shifts close to the central jet as the H/D increase.

This may be because the flow in case of low H/D (0.5 & 1) has more momentum compare to higher H/D, hence the centre jet easily moves the surrounding fluid. The wall jets, thus separated from each other in the impingement plane by the dividing stagnation lines, are shown in Fig.9, by computational surface flow lines for different H/D values of 0.5, 1, 2 & 4.

Figure 10 Shows the Flow structure visualized as traces of oil lamp black on impingement surface. The shape of the dividing stagnation line is like a square around the central jet with protruding curves separating perimeter jets.

The computed and experimentally visualized flow structures qualitatively agree well and hence confirm the correctness of the computation.



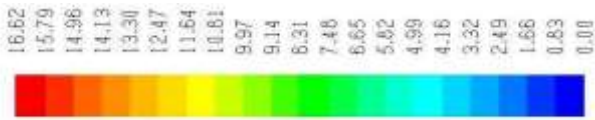


Fig. 8 Path lines Colored by velocity along plane A-A for $Re = 6340$
(a) $H/D = 0.5$, (b) $H/D=1$, (c) $H/D=2$, (d) $H/D=4$

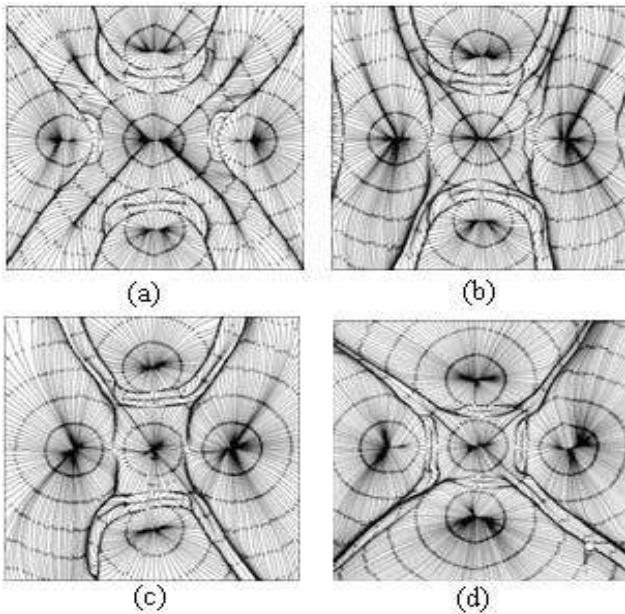


Fig.9 Computed Surface flow lines on the impingement plate, for $Re = 6340$
(a) $H/D=0.5$, (b) $H/D=1$, (c) $H/D=2$, (d) $H/D=4$

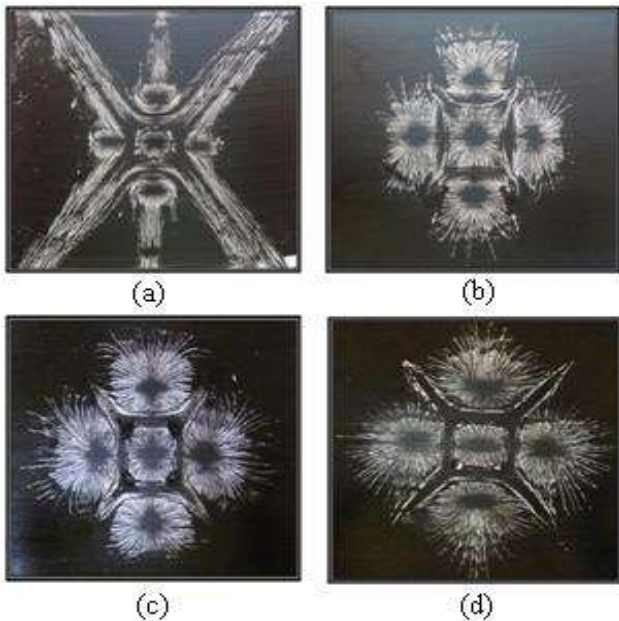


Fig.10 Flow structure visualized as traces of oil lamp black on impingement plate, for $Re = 6340$
(a) $H/D=0.5$ (b) $H/D=1$ (c) $H/D=2$ (d) $H/D=4$

Figure 11 shows the comparison of experimental static pressure distribution on line A-A with computation data. Experimental data and computational data are quantitatively well in agreement with each other and hence the correctness of computation

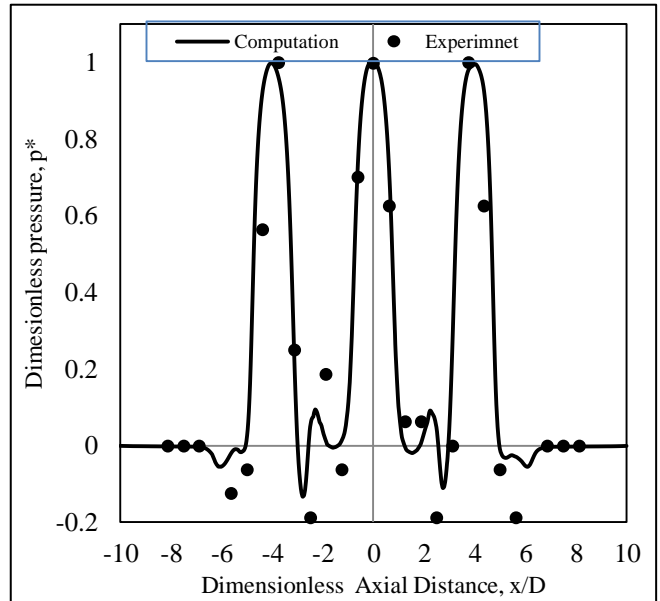


Fig.11 Comparison of static pressure distribution on line A-A, experimental with computation

4.2 Effect of jet-to-Plate Spacing to Jet Hydraulic Diameter Ratio:

Figure 12 shows the variation of non dimensional pressure coefficient P^* distribution with different jet-to-plate spacing to jet hydraulic diameter of slot (H/D) ratio for $Re = 6340$ along line A-A, peak pressure is observed at the point of stagnation of each jet. Up wash fountain for high H/D is more prominent hence larger peaks are observed for higher H/D values. The position of secondary peak depends upon the position of interaction point of wall jet and the size of the central square. Secondary peak moves closer to with increase in H/D .

Figure 13 shows the variation of non dimensional pressure coefficient distribution along line B-B with different H/D .

The behavior of non dimensional pressure coefficient distribution in the stagnation region is similar to the one observed along line A-A. Upwash fountain are more prominent for high H/D hence the secondary peaks observed are larger for high H/D values.

4.3 Effect of Reynolds number

Figure 14 illustrates the dependence of non dimensional pressure coefficient distribution on Reynolds number for $H/D = 2$ on line A-A.

As expected the pressure peaks are higher for high Reynolds number. At any Reynolds number the non dimensional pressure coefficient has the higher value at the stagnation region and reduces radially. Secondary peak is

observed at the second stagnation point where neighboring wall jets collide. Position of secondary peak is independent of Reynolds number.

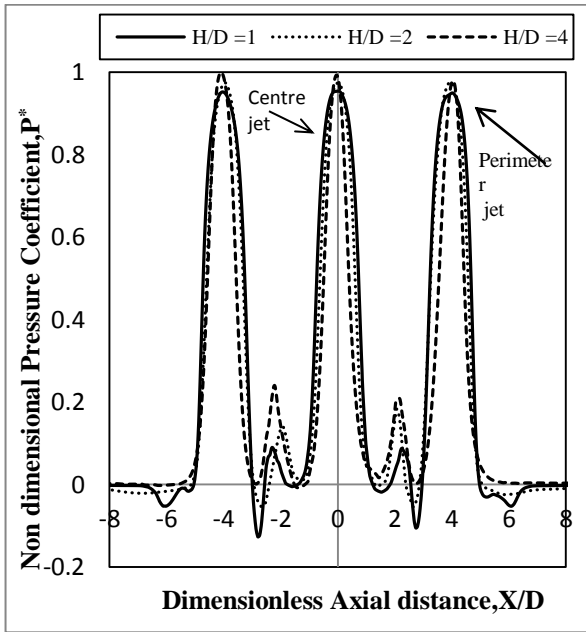


Fig. 12 Non dimensional pressure coefficient distribution along line A-A, for varying H/D, at Re=6340

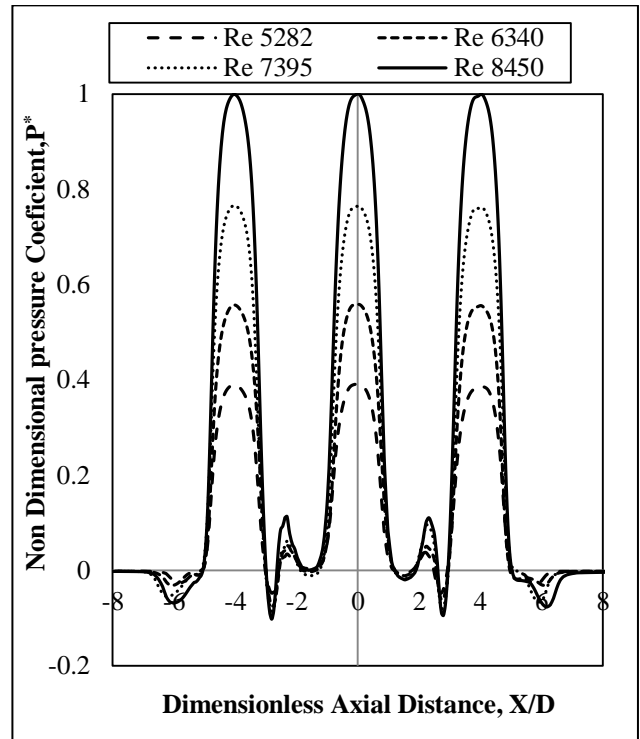


Fig.14 Effect of Reynolds number on Non dimensional pressure coefficient distribution on line A-A for H/D=2

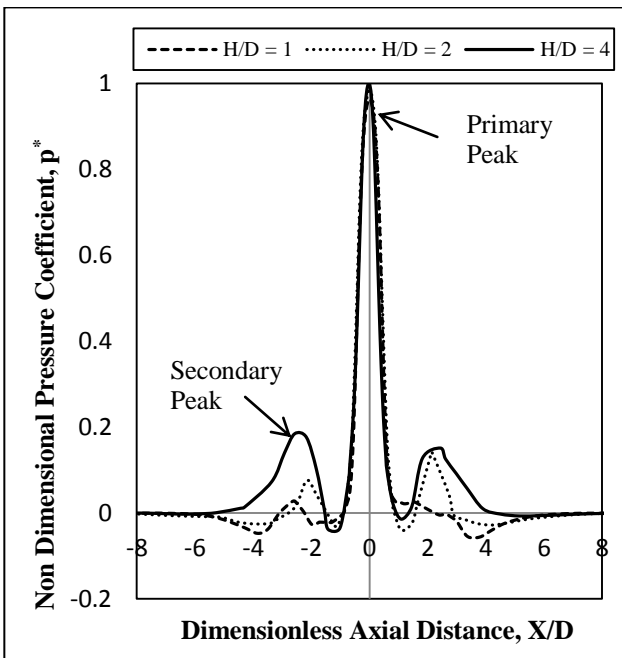


Fig. 13 Non dimensional pressure coefficient distribution along line B-B, for varying H/D, at Re=6340

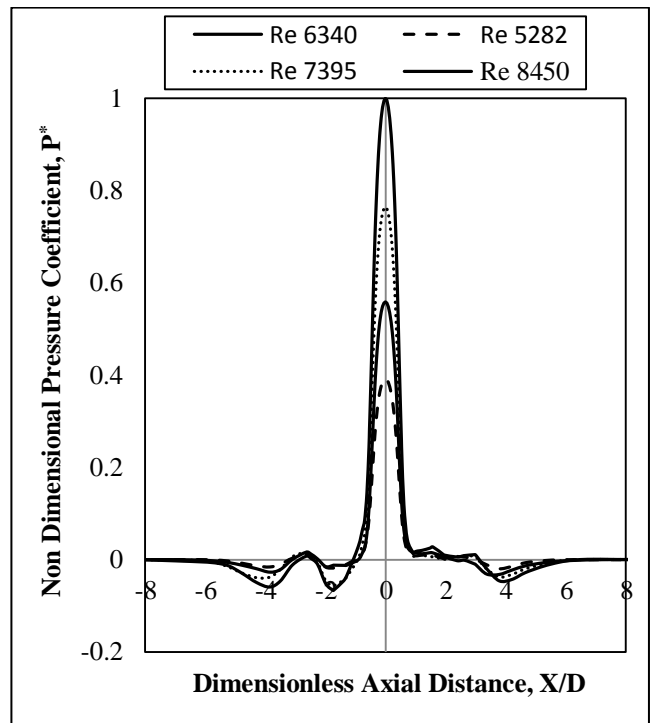


Fig.15 Effect of Reynolds number on Non dimensional pressure coefficient distribution on line B-B for H/D=2

Figure 15 shows the variation of non dimensional pressure coefficient distribution with different Reynolds number along the B-B. The secondary peak formed by the wall jets is higher for high Reynolds number.

The secondary peak formed by the interaction of wall jets is higher for high Reynolds number.

5 CONCLUSIONS

Three-dimensional flow on a flat plate is investigated with five jets impinging on its surface. The following conclusions are drawn from the study:

1. Among the different turbulent models tested, the κ - ω SST turbulence model is found to be a better predictive model for the determination of flow characteristics of impinging jet systems as validation results are good
2. It is observed that the impingement of an upwash fountain on the semi-confining upper plate for low H/D values, with increasing H/D separation point comes closer to the centre jet.
3. Larger pressure peaks are observed for lower H/D and Position of the secondary pressure peaks moves away from centre jet with decrease H/D.
4. Pressure peaks are found to be higher for higher Reynolds number. However, position of the secondary peak is independent of Reynolds number in the range of 5282 to 8450.

NOMENCLATURE

| | |
|----------|---|
| D | Hydraulic Diameter of slot, m |
| H | Jet-to-plate distance, m |
| P^* | Non dimensional pressure Coefficient |
| Re | Reynolds number, $\frac{4m_j}{\pi D \mu}$ |
| V_{oe} | Orifice exit jet velocity, m/s |
| V_z | Vertical velocity, m/s |

Greek Symbols

| | |
|----------|-------------------------------------|
| κ | Turbulent kinetic energy, m^2/s^2 |
| μ | Dynamic viscosity, $kg/m-s$ |
| ν | Kinematic viscosity, m^2/s |
| ρ | Density, kg/m^3 |
| ω | Specific dissipation rate, $1/sec$ |
| ∇ | Gradient operator |

Subscript

| | |
|----|--------------|
| f | Fluid |
| oe | Orifice exit |
| w | Wall |

Abbreviations

| | |
|-----|---------------------------|
| SDR | Specific Dissipation Rate |
| SST | Shear Stress Transport |
| TKE | Turbulent Kinetic Energy |

REFERENCES

- [1] Aldabbagh, L.B.Y., and Sezai, I., 2002, "Numerical simulation of three-dimensional laminar multiple impinging square jets", International Journal of Heat and Fluid Flow, Vol. 23, pp. 509–518.
- [2] Bernhard W., and Sebastian S., 2009, "Multiple Jet impingement - A Review", Int. Symp. On Heat Transfer in Gas Turbine Systems, Turkey.
- [3] Malladi R.Ch.Sastry, A.V.S.S.K.S Gupta and B.V.S.S.S.Prasad, 2011, "Study of fluid flow on a flat plate with three rectangular impinging slots jets" Proceedings of the 38th National Conference on Fluid Mechanics and Fluid Power 2011, MANIT, Bhopal.
- [4] Neil, Z., and Noam L., 2005, "Impingement Heat Transfer: Correlations and Numerical Modeling", ASME Journal of Heat Transfer, Vol. 127, pp. 544 – 553.
- [5] Rajesh Kumar panda and B.V.S.S.S.Prasad, 2011 "Flow visualization and conjugate heat transfer study from Shower head impinging jets" Proceeding of ASME-Turbo Expo 2011, Canada.
- [6] San, J.Y., and M.D. Lai, 2001, "Optimum jet-to-jet spacing of heat transfer for staggered arrays of impinging air jets", International Journal of Heat and Mass Transfer, 44 (21), pp. 3997–4007.
- [7] San, J.Y., Tsou, Y. M., and Chen, Z.C., 2007, "Impingement heat transfer of staggered arrays of air jets confined in a channel", International Journal of Heat and Mass Transfer, Volume 50, pp. 3718-3727